



# Making Archean cratonic roots by lateral compression: A two-stage thickening and stabilization model

Hongliang Wang<sup>a,\*</sup>, Jeroen van Hunen<sup>a</sup>, D. Graham Pearson<sup>b</sup>

<sup>a</sup> Department of Earth Sciences, Durham University, Durham, UK

<sup>b</sup> Department of Earth and Atmospheric Sciences, University of Alberta, Edmonton, Canada

## ARTICLE INFO

### Article history:

Received 1 July 2016

Received in revised form 24 November 2016

Accepted 1 December 2016

Available online 6 December 2016

### Keywords:

Craton formation  
Tectonic shortening  
Gravitational self-thickening  
Craton stabilization  
Secular cooling

## ABSTRACT

Archean tectonics was capable of producing virtually indestructible cratonic mantle lithosphere, but the dominant mechanism of this process remains a topic of considerable discussion. Recent geophysical and petrological studies have refuelled the debate by suggesting that thickening and associated vertical movement of the cratonic mantle lithosphere after its formation are essential ingredients of the cratonization process. Here we present a geodynamical study that focuses on how the thick stable cratonic lithospheric roots can be made in a thermally evolving mantle. Our numerical experiments explore the viability of a cratonization process in which depleted mantle lithosphere grows via lateral compression into a >200-km thick, stable cratonic root and on what time-scales this may happen. Successful scenarios for craton formation, within the bounds of our models, are found to be composed of two stages: an initial phase of tectonic shortening and a later phase of gravitational self-thickening. The initial tectonic shortening of previously depleted mantle material is essential to initiate the cratonization process, while the subsequent gravitational self-thickening contributes to a second thickening phase that is comparable in magnitude to the initial tectonic phase. Our results show that a combination of intrinsic compositional buoyancy of the cratonic root, rapid cooling of the root after shortening, and the long-term secular cooling of the mantle prevents a Rayleigh-Taylor type collapse, and will stabilize the thick cratonic root for future preservation. This two-stage thickening model provides a geodynamically viable cratonization scenario that is consistent with petrological and geophysical constraints.

Crown Copyright © 2016 Published by Elsevier B.V. This is an open access article under the CC BY-NC-ND license (<http://creativecommons.org/licenses/by-nc-nd/4.0/>).

## 1. Introduction

Cratons, the oldest parts of the Earth's lithosphere, owe their longevity and stability to their chemically distinct, highly melt-depleted cratonic roots (Jordan, 1975; Carlson et al., 2005; Burov, 2011; Pearson and Wittig, 2014; Wang et al., 2014). The formation of these roots, however, continues to be debated, and three main endmember hypotheses for the formation of cratonic lithosphere have been proposed (e.g., Pearson and Wittig, 2008; Arndt et al., 2009; Lee et al., 2011). First, a thick, stable mantle lithosphere forms through melting in a large mantle plume head. A second way to form cratons can be the accretion and stacking of segments of oceanic lithosphere. Finally, accretion and thickening of already buoyant arc lithosphere might be capable of producing stable keels. In particular, there has been much debate regarding the relative importance of plume-related melting and vertical accretion versus lateral accretion and thickening by tectonic processes (Griffin et al., 2003; Lee, 2006; Aulbach, 2012; Pearson and Wittig, 2014). The dynamics associated with compressional thickening has long been proposed as an important aspect of cratonization (Jordan, 1978). Recent studies

suggest that vertical tectonics might have played a more important role in the Archean than it does today (Bédard et al., 2003; Sleep, 2005; Sizova et al., 2015). While compressional models of cratonic lithosphere have been long proposed and recently popularised (e.g. McKenzie and Priestley, 2016) there remains, as yet, no in-depth geodynamic model that studies the viability of this process and the timescale over which it may operate, within the framework of modern geodynamical modelling.

The melting depth of the peridotitic protolith is one of the key constraints for the craton formation process (Herzberg, 1999; Canil, 2004; Pearson and Wittig, 2008, 2014; Aulbach, 2012; Lee and Chin, 2014). High pressure (3–6 GPa) melting conditions of craton protoliths obtained from bulk-rock major element studies have been used as evidence for a plume origin (e.g. Pearson et al., 1995; Herzberg, 1999; Aulbach, 2012). However, this approach is vulnerable to the effects that later metasomatic processes have on modifying the bulk compositions used to constrain melting depth (Lee, 2006; Pearson and Wittig, 2008). In contrast, results from mildly incompatible trace elements that are more robust to metasomatic processes argue for a low pressure origin of cratonic peridotite (<3 GPa) (Canil, 2004; Wittig et al., 2008). Lee and Chin (2014) explicitly calculated the temperature and pressure conditions of peridotite melting events through bulk FeO and MgO

\* Corresponding author at: Department of Earth Sciences, University of Bergen, Bergen N5007, Norway.

measurements of the residual peridotite. They concluded that Archean cratonic peridotites were likely formed at melting temperatures of 1400–1750 °C and pressures of 1–5 GPa (30–150 km), and subsequently transported to depths of 3–7.5 GPa (90–200 km), where they cooled and stabilized.

Cooper and Miller (2014) studied the thickening of buoyant residual mantle material over a mantle down-welling using geodynamical modelling and suggest that the observed seismic ‘mid-lithospheric discontinuities’ might be explained by localized deformation during the thickening phase of the cratonic lithosphere. The driving force for this vertical movement of depleted peridotite is either an external tectonic force or internal gravitational forces. Studies of the secular thermal evolution of the cratonic lithosphere demonstrate that the often proposed isopycnic state of cratonic lithosphere is an inherently ephemeral phenomenon due to the evolution of negative thermal buoyancy (Eaton and Claire Perry, 2013). Laboratory experiments on the physical properties of depleted mantle rocks indicate that subcratonic mantle formed shallower than ~110 km is negatively buoyant with respect to adiabatic mantle (Schutt and Leshner, 2006), which suggests that such residues are capable of gravitationally-driven vertical movement.

Both petrological evidence and geophysical constraints indicate that vertical movement of lithosphere is likely during craton formation. This suggests that shortening and thickening of depleted mantle material may be common, and might provide a viable geodynamical scenario for the cratonization process. However, the controlling factors that enable both initial thickening and subsequent, long-term stabilization of cratonic lithosphere remain unclear and have yet to be fully explored. In particular how the cratons evolve to their stable roots from an unstable thickening phase, without under-going Rayleigh-Taylor collapse (e.g. Houseman and Molnar, 1997) requires more investigation. Therefore, in this study, we present a set of numerical experiments that investigate how cratons might have grown to their current thicknesses, via lateral compression, within a thermally evolving mantle, while preserving long-term stability. We explore the potentially important model parameters related to craton thickening and stabilization.

## 2. Model description

### 2.1. Governing equations

We use a Cartesian version of the finite element code Citcom (Moresi and Solomatov, 1995; Zhong et al., 2000; van Hunen et al., 2005) to solve the incompressible flow with Boussinesq approximations. The non-dimensional governing equations for mass, momentum, energy conservation are:

$$\nabla \cdot \mathbf{u} = 0, \quad (1)$$

$$-\nabla P + \nabla \cdot (\eta(\nabla \mathbf{u} + \nabla \mathbf{u}^T)) + (RaT - Rb_i C_i) \mathbf{e}_z = 0, \quad (2)$$

$$\frac{\partial T}{\partial t} + \mathbf{u} \cdot \nabla T = \nabla^2 T + Q_0. \quad (3)$$

A standard non-dimensionalisation is used with  $x = x'h$ ,  $t = t'h^2/\kappa$ ,  $\eta = \eta'\eta_0$ ,  $T = (T' + T_0)\Delta T$ , where the primes of the non-dimensional parameters are dropped for clarity in the above equations. The dimensional physical parameters are listed and explained in Table 1. The thermal and compositional Rayleigh number  $Ra$  and  $Rb_i$  are defined as:

$$Ra = \frac{\alpha \rho_0 g \Delta T h^3}{\kappa \eta_0}, \quad (4)$$

$$Rb_i = \frac{\delta \rho_i g h^3}{\kappa \eta_0}. \quad (5)$$

**Table 1**  
Symbols, units and default parameters.

Symbol	Description	Default value and units
A	Rheological pre-exponent (dislocation)	$1.1 \times 10^5, 2.21 \times 10^{-4}$ [MPa <sup>-n</sup> s <sup>-1</sup> ]
B	Rheological pre-exponent (diffusion)	$5.81 \times 10^{-4}$ [MPa <sup>-1</sup> ]
E	Mantle activation energy	530 (ds), 375 (df) [kJ/mol]
Ec	Crust activation energy	260 (ds), 375 (df) [kJ/mol]
g	Gravitational acceleration	9.8 [m/s <sup>2</sup> ]
h	Model height	400 [km]
c <sub>p</sub>	Thermal capacity	1250 [J kg <sup>-1</sup> K <sup>-1</sup> ]
n	Rheological power law exponent	3.5, 3.4 (ds), 1 (df) [-]
P	Pressure	[Pa]
R	Gas constant	8.3 [J/mol]
Ra	Thermal Rayleigh number	$1.1228 \times 10^6$ [-]
Rb <sub>i</sub>	Compositional Rayleigh number <sup>a</sup>	$3.7632 \times 10^6,$ $1.9757 \times 10^5$ [-]
T	Temperature	[°C]
ΔT	Temperature drop over model domain	1350 [°C]
ε̇	Strain rate	[s <sup>-1</sup> ]
α	Thermal expansion coefficient	$3.5 \times 10^{-5}$ [K <sup>-1</sup> ]
η <sub>0</sub>	Reference viscosity	10 <sup>20</sup> [Pa·s]
η	Viscosity	[Pa·s]
κ	Thermal diffusivity	10 <sup>-6</sup> [m <sup>2</sup> /s]
ρ <sub>m</sub>	Mantle density	3300 [kg/m <sup>3</sup> ]
Δρ <sub>1</sub>	Density difference of crust and mantle	600 [kg/m <sup>3</sup> ]
Δρ <sub>2</sub>	Maximum density change due to depletion	31.5 [kg/m <sup>3</sup> ]
Q <sub>0</sub>	Present day mantle radioactive heating	0.02 [μW/m <sup>3</sup> ]
C <sub>i</sub>	Composition field	0–1 [-]
τ <sub>0</sub>	Yield stress at the surface	40 [MPa]
τ <sub>max</sub>	Maximum yield stress	400 [MPa]
μ	Friction coefficient	0.6 [-]

<sup>a</sup>  $3.7632 \times 10^6$  and  $1.9757 \times 10^5$  are the compositional Rayleigh numbers for crust and cratonic root, respectively.

We use a composite rheology of dislocation and diffusion creep which assumes that the melt-depleted mantle is dry and therefore more viscous than the undepleted mantle (Hirth et al., 2000; Karato, 2010). The rheology setup is similar to Wang et al. (2015), but we ignore the pressure dependence of the rheology in order to reduce the model complexity and focus on lithosphere dynamics. The composition-dependent viscosities for dislocation creep and diffusion creep are defined as:

$$\eta_{dl} = A \left( \frac{-1}{n} \right) \dot{\epsilon} \exp \left( \frac{E}{nRT} \right) \times \Delta \eta, \quad (7)$$

$$\eta_{df} = B \exp \left( \frac{E}{RT} \right) \times \Delta \eta^n \quad (8)$$

In which  $\Delta \eta$  is the strengthening that results from melt depletion. In addition, we apply a yielding mechanism (van Hunen and Allen, 2011) to consider the brittle yielding of strong lithosphere during the imposed shortening process:

$$\eta_y = \frac{\min(\tau_0 + \mu P, \tau_{\max})}{\dot{\epsilon}}, \quad (9)$$

with the description of the rheological parameters listed in Table 1. Therefore, the effective viscosity is defined as:

$$\eta_{eff} = \min(\eta_{dl}, \eta_{df}, \eta_y). \quad (10)$$

In contrast to the mantle, the crust is assigned a weaker rheology in order to take into account the potentially important effects of relatively weak and buoyant crust. The rheological parameters for the crust and mantle are presented in Table 1. Melt-depleted lithosphere is commonly assumed to be dehydrated, and therefore more viscous than normal lithosphere (Hirth and Kohlstedt, 1996). A strengthening factor of  $\Delta \eta = 3$  is used in Eqs. (7) and (8) for the

depleted cratonic mantle lithosphere (Wang et al., 2014), while all other materials have  $\Delta\eta = 1$ . Due to the non-linear stress-strain rate relationship used in the non-Newtonian rheology, the effective compositional viscosity increase depends on the ambient stress or strain rate. In this study, we use a ‘constant strain rate’ value of  $\Delta\eta = 3$ , corresponding to a ‘constant stress’ value of  $\Delta\eta^n = 46.8$ , for  $n = 3.5$ . The choice of  $\Delta\eta = 3$  is based on the outcomes of our previous studies (Wang et al., 2014, 2015) and is within the range of acceptable values obtained from laboratory measurements (Hirth and Kohlstedt, 1996; Karato, 2010; Fei et al., 2013).

## 2.2. Model setup

The computational domain is 400 km deep and 1600 km wide, with initially depleted mantle material located between  $x = 200$  and 1400 km, and with a 20-km thick crust. This model setup is illustrated in Fig. 1, together with the mechanical and thermal boundary conditions. A free-slip boundary condition is used on the surface, which allows for shortening of the lithosphere. The bottom boundary is open to allow material flow in and out of the model domain, so that the deformation of the cratonic root is least affected by the bottom boundary. A velocity profile ( $v = V_s$  at the surface), that assumes uniform shear stress and zero net flux, is imposed at the side boundaries for a given period (see Fig. 1 and below), and moves the lithosphere towards the center of the domain. This process mimics a time-limited tectonic shortening event. We control the amount ( $L_s$ ) of the lithosphere flow into the domain from the side boundaries by changing the imposed in-flow speed  $V_s$  and duration  $t_s$ . The amount/length of lithosphere that flows into the domain is counted into the total original length ( $L + L_s$ ) of the lithosphere. During the shortening event, the original length of the lithosphere ( $L + L_s$ ) shortens to a length of  $L$ . Then the shortening factor of the lithosphere can be calculated after (Mckenzie and Bickle, 1988) as:

$$\beta = \frac{L}{L + L_s} = \frac{L}{L + 2 \times V_s \times t_s} \quad (11)$$

where  $L = 1600$  km is the width of the model domain.  $\beta = 0.62$  in the Reference Model R (see Table 2). Although isostatic balance is implicitly maintained through normal stresses acting on the free-slip surface boundary, topography is not explicit in the models. Therefore, surface erosion processes are also not considered in this study, which is probably one of the main model limitations, since this process might affect crustal thickness over long timescales.

We ignore any initial thermal differences between the depleted mantle and normal mantle, and use a 30 Myr half-space cooling age for the initial thermal structure of the whole lithosphere, as shown in Fig. 1. Considering the intense radiogenic heating within continental

**Table 2**  
Comparison of parameters in all discussed models.

Model	Shortening factor	Shortening velocity (cm/yr)	Basal cooling rate ( $^{\circ}\text{C}/\text{Gyr}$ )
SF1	1	0	100
SF2	0.73	1	100
R	0.62	1	100
SF3	0.5	1	100
SR1	0.62	2	100
SR2	0.62	1.43	100
SR3	0.62	0.5	100
SR4	0.62	0.25	100
SC1	0.62	1	50
SC2	0.62	1	0

crust during the Archean (Mareschal and Jaupart, 2006), this young thermal age of lithosphere is appropriate. As we aim to model the thickening of cratonic root in the hotter Archean era, we use an initial mantle potential temperature of  $1550$   $^{\circ}\text{C}$  in the models, which is within the range of petrological estimates (Herzberg et al., 2010; Condie et al., 2016). The first-order effect of mantle secular cooling is included by a constant cooling rate  $\lambda$  ( $^{\circ}\text{C}/\text{Gyr}$ ) for the basal temperature boundary condition:

$$T_b = T_{b0} - \lambda t \quad (12)$$

Secular cooling of the Earth’s mantle ( $\lambda$ ) has been estimated to be  $50$ – $100$   $^{\circ}\text{C}/\text{Gyr}$  (e.g. Grove and Parman, 2004; Michaut and Jaupart, 2007; Herzberg et al., 2010). We use  $\lambda = 100$   $^{\circ}\text{C}/\text{Gyr}$  in the reference model, but we also explore the effects of different cooling rates in Section 3.2.3.

Compositional buoyancy due to melt depletion in the lithospheric mantle plays an important role in the presented models. The effect of melt depletion on the mantle density has been suggested to be smallest at pressures between 1 and 3 GPa, where 20% melt removal results in only a 0.42%–0.46% density reduction, compared to 0.90%–1.14% at pressures between 3.5 and 4.5 GPa (Fig. 1) (Schutt and Leshner, 2006). The amount of depletion within the lithospheric profile, however, is likely to decrease with depth. We combine these contrasting effects, and assign an effective compositional density reduction due to melt depletion as shown in Fig. 1, A2. This amounts to a maximum density reduction of  $31.5$   $\text{kg}/\text{m}^3$  (0.95%) in our models, consistent with experimental data at pressures around 3.5–4.5 GPa (Fig. 1, A3, Schutt and Leshner, 2006).

Apart from the rheological and density effects of the crust, its high radiogenic heat production during the Archean may also play a role in the dynamics of lithospheric shortening. We use a present-day crustal radiogenic heat production  $Q_0 = 0.02$   $\mu\text{W}/\text{m}^3$ , a constant ratio of 30:1

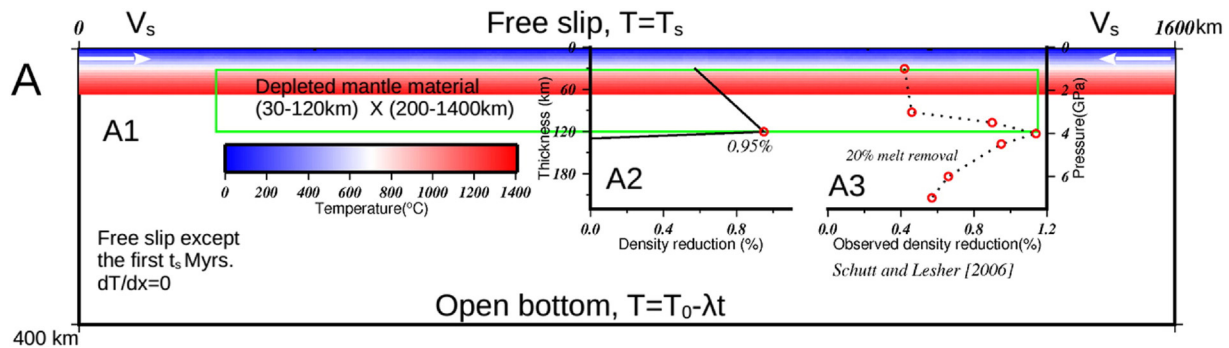


**Fig. 1.** Model setup of the cratonic root, including mechanical and thermal boundary conditions, initial thermal condition and initial chemical profile. The initial compositional profile  $C_2$  (depletion related), as plotted in the left inset diagram A2, increases from 0.6 to 1 between 30 km and 120 km. The chemical buoyancy reaches its maximum value at 120 km, where it is 0.95% less dense than typical the  $3300$   $\text{kg}/\text{m}^3$  reference density for undepleted peridotite. For comparison, the depth-dependent depletion effect for 20% melting on the density of mantle peridotite from (Schutt and Leshner, 2006) is plotted in the right inset diagram A3.

of the radiogenic heating between the crust and mantle, and an Archean heat production of 3 times the present-day value with a half-life of 1.8 Gyr for both the crust and mantle. These values fall within the suggested ranges for the Earth's thermal evolution and heat production values (Michaut and Jaupart, 2007; Michaut et al., 2009).

### 3. Results

#### 3.1. Cratonic thickening processes

Figs. 2 and 3 show the general thickening process of the cratonic root in the Reference Model R (Table 2) with temperature, composition, velocity and viscosity evolution. Craton thickening begins with an initial 50 Myr of compressive shortening, but after this period of externally imposed tectonic shortening, thickening continues, and eventually the initially thin layer of depleted mantle material slowly grows into a thick cratonic root over a total duration of several 100 Myr. At that point, the lithosphere in the model has reached an equilibrium stage, in which compositional and thermal buoyancy has become similar, and diffusive cooling from the surface and convective heating at the base of the lithosphere approximately cancel out. To illustrate the dynamics of this thickening process, the evolution of the depleted root is monitored in several ways. In Fig. 2, the area with  $T > 1400$  °C is removed, so that the temperature images effectively show the (thermally defined) lithosphere. Hereafter, we refer the areas shown in the Fig. 2 by the temperature image and chemical contour (green) as the thermal root and chemical root, respectively. The thickness of the cratonic root is monitored through time as the average depth extent of the chemical root in the central region between  $x = 550$  km and  $x = 1050$  km. We

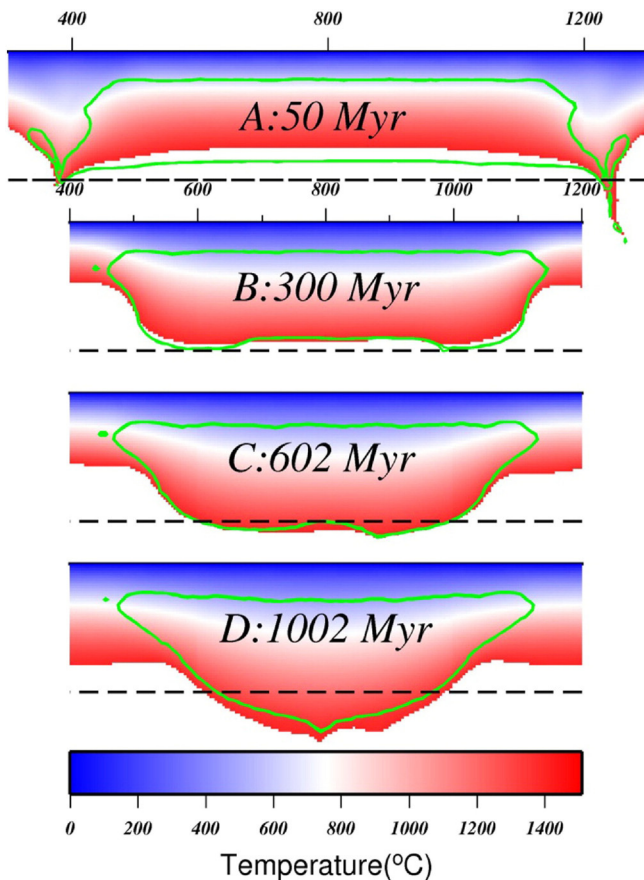


**Fig. 2.** The thickening process of the cratonic root in Reference Model R. Colours indicate the temperature distribution. Temperatures above 1400 °C (taken as the thermal lithosphere boundary in this study) are removed to clarify the lithosphere thickening process. The green contours outline the chemical roots.

also calculate the remaining root in the cratonic lithosphere as the percentage of the original root volume, to monitor the erosion of the root. The time evolution of Reference Model R is shown in Fig. 4 (red line) in terms of the average chemical root thickness (Fig. 4A) and remaining root percentage (Fig. 4B).

The thickening process consists of two separate stages. The first stage is a direct consequence of the externally imposed compressional tectonic shortening. As constant inward velocities are imposed at both side boundaries, the depleted root material in the middle of the domain is pushed downwards, which causes the initial shortening and thickening of the cratonic root (Figs. 2A and 3A). As the depleted mantle material is compositionally buoyant and more viscous compared to normal mantle, it resists this thickening process, which results in more thickening at the edge than at its interior (Fig. 2A). The depleted root material is thickened from ~130 km (including the thin transition layer) to about ~173 km depth within the first 50 Myr, while the thermal root is significantly thinner (Figs. 2A and 3A). After the imposed compressional thickening of Stage 1, the resultant thermal and chemical structure is by no means in steady state. When the thickened root cools and becomes denser, its negative thermal buoyancy starts to exceed the inherent chemical buoyancy and results in further thickening (Stage 2), as shown by the evolutions of i) temperature (Fig. 2B–D), ii) composition (Fig. 3B–D) and iii) viscosity (Fig. 3F–H) evolution. During this phase, the chemical root grows from ~173 km at  $t = 50$  Myr to ~209 km depth at  $t = 600$  Myr (red line in Fig. 4A), and the thermal root grows to approximately the same depth as the chemical root (Figs. 2A–C and 3A–C). This self-driven gravitational thickening is controlled simply by the cooling of the cratonic lithosphere and therefore has a similar time-scale to that of the thermal diffusive cooling of the lithosphere. Both of the two thickening stages involve some recycling of the root material as illustrated in Fig. 4B (red line): ~20% during the compressive thickening regime and ~6% during the self-driven thickening regime. The cratonic root continues to slowly thicken and shorten as a result of deformation after 600 Myr (Fig. 2C–D), but almost no chemical root recycling occurs (Fig. 3B). This indicates that the buoyancy and high viscosity of the now thickened depleted root prevents the development of a significant Rayleigh–Taylor instability and stabilizes the root during and after the major gravitational thickening.

#### 3.2. Model parameter sensitivity

In order to investigate how robust the results in the Reference Model R are, a series of “sensitivity testing” model calculations are performed, in which some of the most influential model parameters are varied.

##### 3.2.1. Shortening factor

First, the effects of different shortening factors  $\beta$  are investigated, by changing the duration of shortening and thus the length of the lithosphere that flows into the domain. The same 1 cm/yr inflow speed is imposed at the boundary but with different shortening durations of 0 Myr (SF1), 30 Myr (SF2), 50 Myr (R) and 80 Myr (SF3), resulting in respective shortening factors of 1, 0.73, 0.62 and 0.5 (Table 2). Fig. 4 illustrates the evolution of the (compositional) thickness and the remaining root volume in these models. Without any imposed shortening (Model SF1), no self-driven gravitational thickening of the depleted mantle occurs either (Fig. 4A). Although most of the depleted material survives for at least 1 Gyr in this case (green line in Fig. 4B), a thick cratonic root that approaches the observed thickness of modern-day cratons, is not formed. In Model SF2 (1 cm/yr  $\times$  30 Myr), a slow self-driven thickening stage follows the tectonic shortening stage and helps to form a lithosphere root with an approximately steady-state depth of ~160 km (blue line in Fig. 4A). However, 160 km is significantly thinner than the thicknesses of most present-day cratons (e.g. Gung et al., 2003; Priestley and McKenzie, 2013). From Fig. 4A, it is clear that the gravitational thickening (Stage 2) is significantly larger in Reference Model R (~43 km) than in Model SF2 (~10 km). This illustrates that substantial

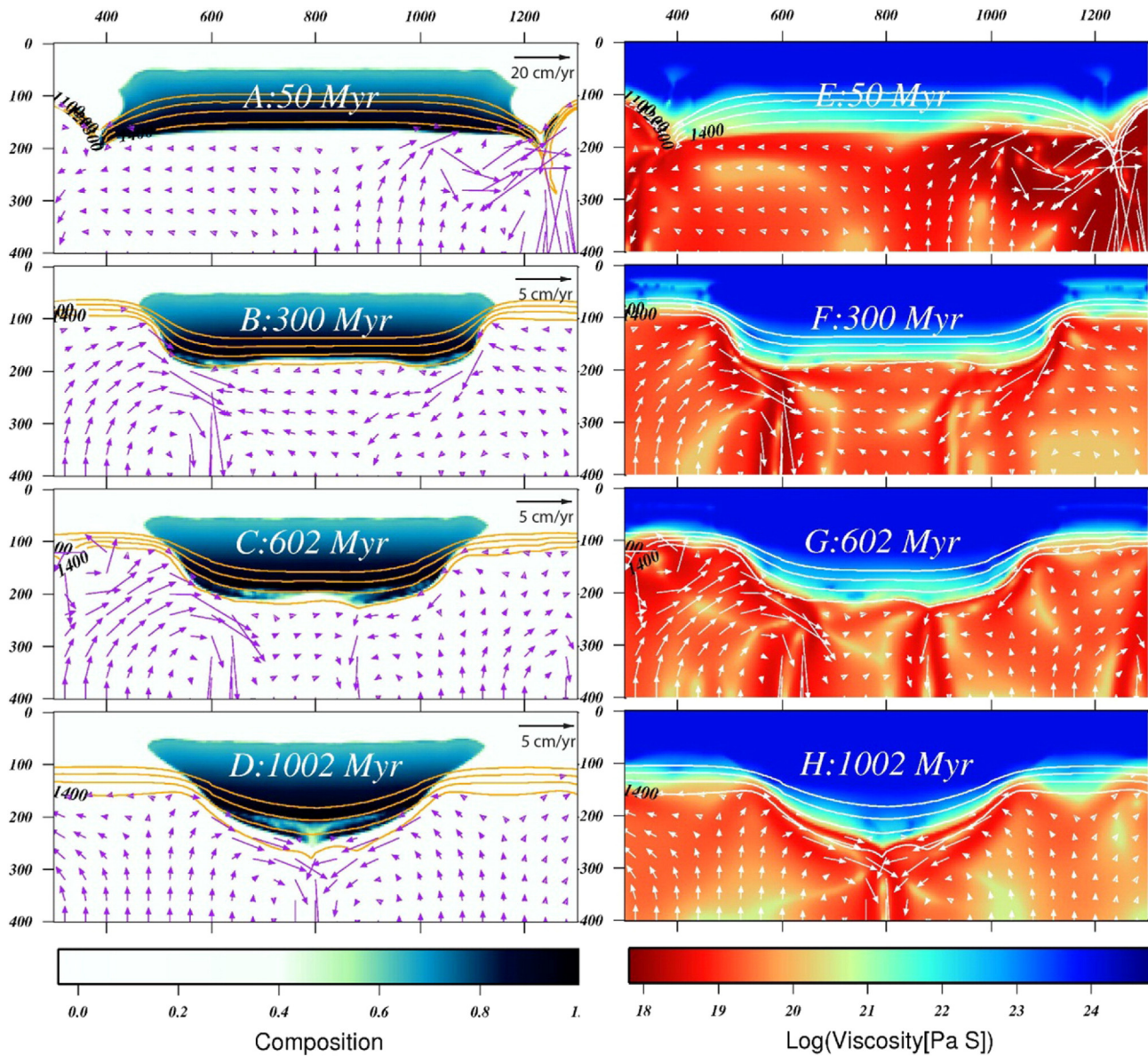


**Fig. 3.** The evolutions of the chemical root (A–D) and viscosity (E–H) during the thickening process of the cratonic root in Fig. 2. The arrows show the velocity field at each time point. The isotherms of  $T = 1100$  °C, 1200 °C, 1300 °C, 1400 °C are also plotted.

initial thickening and shortening of depleted lithospheric mantle material is essential for the development of subsequent late-stage gravitational thickening of the cratonic root.

Imposing significantly more shortening than in the reference model leads to different dynamics, as shown by Model SF3 (Figs. 4 and 5A–C). In that case, the depleted material is pushed down to a depth of >240 km within 80 Myr. Late-stage additional thickening does not occur in this model, but, instead, significant thinning of the root occurs (orange lines in Fig. 4) due to the fact that the root is too buoyant to stay at the increased depth (unstable structure of the thick root). The convex upward shape of both the compositional and thermal roots in Fig. 5A illustrates the resistance of the depleted buoyant root against the imposed shortening. As the root cools down through time, it becomes eroded from the side to the center and the lower thermal and compositional surfaces slowly convert to a convex downward form (Fig. 5B). Unlike in previous models, the chemical root undergoes significant instability and recycling (Figs. 4B and 5A–C) before it has the chance to cool down sufficiently to form a stabilizing thermal boundary, as it does in Reference Model R. Instead, more and more root material is

recycled (orange line in Fig. 4B) and the root becomes progressively smaller (Fig. 5A–C) over time, which does not form a stable craton.

### 3.2.2. Shortening rate

Next, we investigate the effects of different shortening rates by imposing the same shortening amount as in the Reference Model R ( $\beta = 0.62$ ). As listed in Table 2, these different shortening rates lead to shortening durations of 25, 35, 50, 100, and 200 Myr in models SR1, SR2, R, SR3, and SR4 (Table 2), respectively. Although the imposed in-flow rate varies by about an order of magnitude among the models, all of these models form a cratonic root of ~200 km or thicker (Fig. 6). Except for Model SR1, the recycling of the root during craton thickening generally shows a positive correlation with the shortening rate, with slower shortening resulting in less recycling of the root (Fig. 6B). This is explained by the stress field imposed by the tectonic shortening. Faster shortening induces stronger stress-weakening effects on the root material, which, in turn, leads to more delamination of this root. A sudden drop in the amount of remaining root at the end of the tectonic shortening stage in Model SR1 SR2, R, and SR3 in Fig. 6B is caused

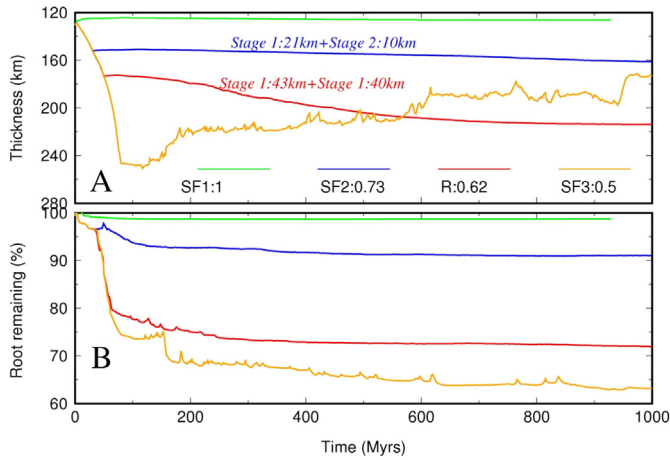


**Fig. 4.** A) Secular evolution of modelled cratonic roots, measured as their average thickness between  $x = 550$  km and  $x = 1050$  km in models with different shortening factor  $\beta$ . The thickness is calculated by using the compositional (rather than thermal) root definition in order to exclude any effects of secular cooling. The two thickening stages in Model R and SF2, tectonic compressive thickening and gravitational thickening, are clearly marked by a kink in the curves. B) Volumetric percentage of remaining root material over time to illustrate the amount of recycling into the underlying upper mantle of chemical root material.

by the delamination of root material in these models. This phenomenon does not occur in Model SR4, which experiences very slow shortening. However, Model SR1, which has the fastest shortening rate, preserves more root material than most other models and indicates another regime of shortening dynamics, as elaborated below.

In order to show the differences in shortening dynamics between the different models, the chemical root geometry in Models R, SR1 and SR4 is plotted for a model time around 600 Myr in Fig. 5D–F. Within the shortening time of 25 Myr in Model SR1, part of the root material starts to delaminate from the main root but has not cooled down enough yet to become sufficiently dense to detach completely into the

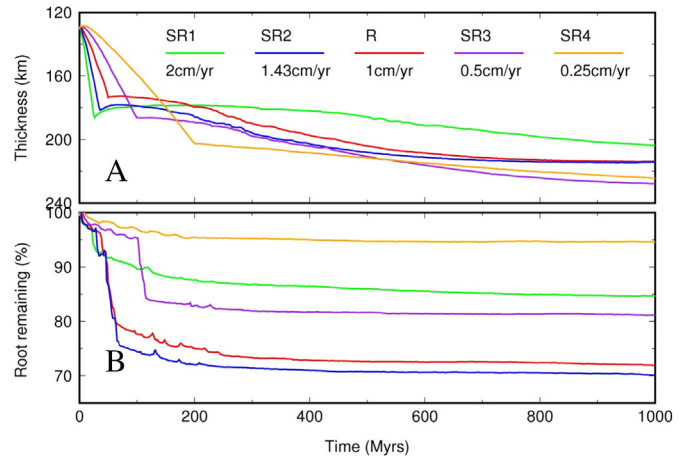


**Fig. 6.** The thickening and recycling of cratonic root material in models with different shortening rates (Model SR1, SR2, R, SR3, SR4). The same shortening factor ( $\beta = 0.62$ ) is applied in these models, which results in different shortening periods (25 Myr, 35 Myr, 50 Myr, 100 Myr, 200 Myr, respectively).

underlying asthenosphere. Instead, it resides at either side of the main cratonic root, and buffers the main root from edge-driven erosion (Fig. 5E), which prevents it from significant gravitational thickening. The root in the fast shortening Model SR1 is therefore slightly thinner (Fig. 6A), but preserves more root than in the slower-shortening Models SR2, R, or SR3 (Fig. 6B). On the other hand, Model SR4, with the slowest shortening rate, preserves almost 95% of its original depleted mantle area without any sudden losses of root material (Fig. 6B). In this case, the root has enough time to cool down, and stress weakening induced by tectonic-shortening is insufficient to delaminate any significant amount of root material. These results illustrate that the tectonically induced shortening rate during craton formation plays an important role in the thickening dynamics and the recycling of the cratonic root.

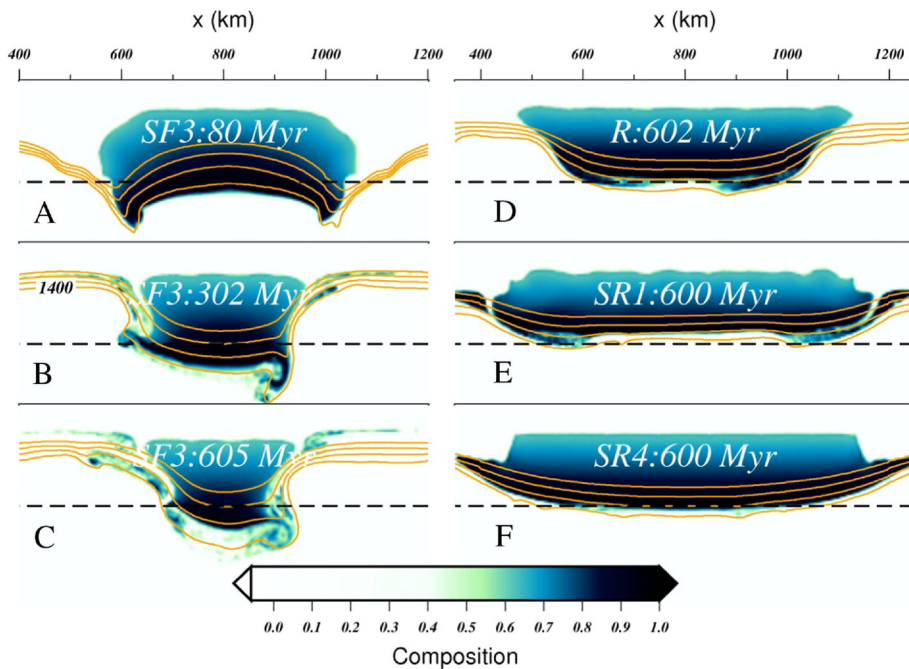


**Fig. 5.** A)–C) Chemical root images of Model SF3 at 80 Myr (A), 302 Myr (B), 605 Myr (C). Significantly more tectonic shortening Stage 1 leads to an unstable thermo-chemical structure, in which the root becomes smaller over time. D)–F) Chemical root image of Model R (D), SR1 (E) and SR4 (F) at around 600 Myr. Strong yielding in Model SR1 (E) induces an undulating boundary at the top of the chemical root. The orange curves are the isotherm of  $T = 1100$  °C, 1200 °C, 1300 °C, 1400 °C, respectively. The dashed lines indicate depth intervals of 200 km.

### 3.2.3. Secular cooling

In our Reference Model R, the basal temperature reduces by 100 °C/Gyr in order to mimic the effects of secular cooling of the mantle. In this section, we compare models with different cooling rates (Table 2) and show how this affects the craton thickening and stabilization process. Fig. 7 shows the thickness and root volume evolution of three models with cooling rates of 100 °C/Gyr (Model R), 50 °C/Gyr (Model SC1), and 0 °C/Gyr (i.e. no cooling, Model SC2). While Models R and SC1 remain stable even after  $t = 1$  Gyr, SC2 without basal cooling (0 °C/Gyr) has a quiet period until  $t = 1$  Gyr, but then starts to show significant perturbations as observed in both the root thickness (Fig. 7A) and root volume (Fig. 7B). The cratonic root is clearly thinned and recycled during this active period, indicating substantial root dynamics. The average velocity of the compositional root (Fig. 7C) shows that the cratonic root in Model SC2 becomes dynamically active after 1 Gyr, such that it approaches the average velocity of the whole computational domain (thick, red). The root in Model R becomes less active (and thus more stable) over the same time period, while the root in Model SC1 (50 °C/Gyr) displays a relatively constant degree of activity through time.

To further illustrate the nature of the instabilities in Model SC2, its root dynamics are monitored and illustrated over a short 36-Myr timespan from 1409 to 1445 Myr (Fig. 8). The core of the root displays minimal change of shape within this short period, as indicated by the isotherms (1100 °C–1300 °C). However, during this period, some of the marginal root material vigorously moves around cyclically in a time-scale of 30–40 Myr. Each cycle results in some of the root material eroding away (Fig. 8B). Unlike a more classical Rayleigh-Taylor instability of the thickening lithosphere (Houseman and Molnar, 1997) in which the root material typically never returns, this instability of the compositionally buoyant root shows an oscillatory behaviour. Similar oscillatory instabilities were also found in both laboratory studies (e.g. Jaupart et al., 2007) and independent numerical modelling studies (e.g. Wang et al., 2015).

## 4. Discussion

Our numerical models show that craton roots of similar thickness to Earth's cratons (>200 km) can be formed successfully from a relatively thin depleted mantle lithosphere layer (30–120 km), through a two-stage thickening and stabilization process. The starting thickness is no greater than the thickness of depleted buoyant oceanic lithosphere expected to form at a hot mid-ocean ridge for instance (e.g., Herzberg et

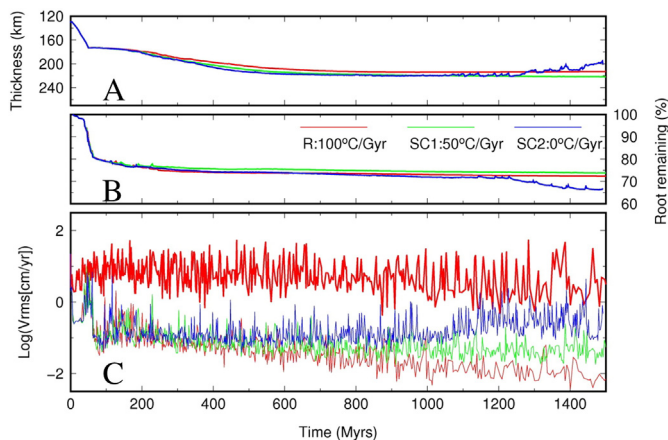


**Fig. 7.** Thickness (A), remaining root (B) and root-mean-square velocity (C) of the cratonic root material in models with different secular basal cooling rates. Whereas Model R (100 °C/Gyr) and SC1 (50 °C/Gyr) remain stable indefinitely, the cratonic root in Model SC2 which has no basal cooling starts to show significant thinning and recycling of the root material after ~1 Gyr. The thick red line is the average vrms of the whole model domain in Reference Model R.

al., 2010). In this scenario, cratonization is triggered by tectonic shortening, which is then followed by a period of internally-driven gravitational thickening, as illustrated in Fig. 9. Significant downward movement and cooling of cratonic root material occurs during craton formation, a result that is consistent with the observation that cratons are typically thicker and colder than its protolith (Lee and Chin, 2014). Below, we further discuss the viability and limitations of this cratonization model in relation to two important aspects: craton formation and craton stabilization.

### 4.1. Formation of cratons

The initial, tectonically driven, compressive thickening phase in our proposed cratonization process plays an essential role in the initialization of the thickening process (Fig. 9). Without enough initial compressive thickening of the depleted mantle material, the subsequent self-driven thickening of the root will not take place (Model SF1) or cannot form a substantial cratonic root (Model SF2). However, thickening is not necessarily achieved by the simple shortening process that is used in this study. Sleep (2005) suggested that cratonic lithosphere is formed by processes analogous to modern tectonics. Indeed, cratonization might involve phenomena such as subduction accretion, lithospheric underplating, or continental collision, all of which require tectonic, localized deformation, processes that are not accurately captured by our relatively simple model setup. Studies of modern collision tectonics have shown that the plate convergence is accommodated by a variety of mechanisms (Toussaint et al., 2004; Burov and Yamato, 2008), including shortening by pure-shear thickening or folding. The most striking, present-day example of this is the formation of the Tibetan plateau, whose lithosphere has undergone several hundred kilometres of shortening over 10s of Myr (DeCelles, 2002; Tian et al., 2013). McKenzie & Priestley (2016) have recently proposed that the Tibetan Plateau and its underlying root is the best modern example of a craton in the early stages of its formation. Whether the Tibetan plateau will eventually form a stable craton or not under the present-day mantle conditions is beyond the scope of this study, but it provides a real example of the time and length scales of compressive thickening as envisioned in our models. Regardless of the tectonic manifestation, craton formation requires lithosphere to gradually develop strength and a balance between compositional and thermal buoyancies such that deformable lithosphere can grow into virtually indestructible cratons.

Although our models show that the slow, prolonged tectonic shortening preserves more cratonic root than fast, short-lived tectonic thickening (Fig. 6), compressive shortening events lasting 100s of Myr (Models SR3 and SR4) are not documented in the geological record. This suggests that fast, short-lived shortening (10s of Myr, e.g., Models SR1, SR2 and R) that involve substantial recycling (~30%) of the root probably provides a more realistic craton formation scenario, especially in the Archean Earth where plate speeds could have been faster (van Hunen and van den Berg, 2008). The high stresses associated with the rapid shortening of Model SR1 lead to significant localized yielding of the lithosphere, and the associated localized crustal thickening induces an undulating boundary on the top of the root (Fig. 5E). This behaviour is similar to that described for the localized thickening of cratonic lithosphere by Cooper and Miller (2014), who proposed that the variable depth of the observed mid-lithospheric seismic discontinuities within cratonic lithosphere might be introduced by the thickening phase during the craton formation.

Therefore, we propose a two-stage development of cratons, wherein the second stage - gravitational thickening - lasts for 100s of Myr (Fig. 6), and is driven by the cooling and growth of the negative thermal buoyancy of the root material as a result of the compressive thickening and subsequent diffusive cooling. Mareschal and Jaupart (2006) suggested that the thermal field of cratonic lithosphere might remain in disequilibrium for ~1–2 Gyr after root formation, which is broadly consistent with the ~600 Myr of continued thickening displayed by our

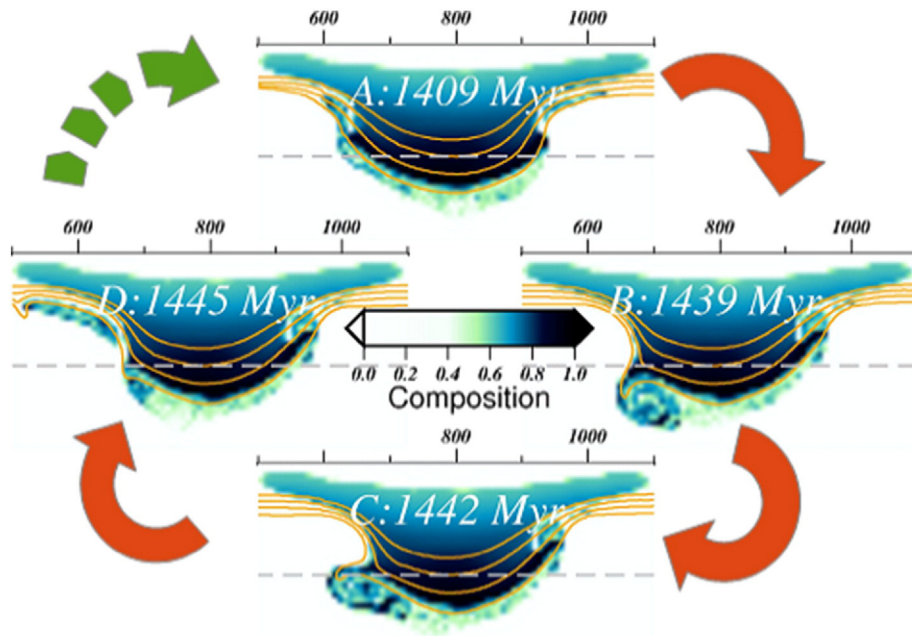


**Fig. 8.** Illustration of the oscillatory instability of the cratonic root after 1 Gyr in Model SC2 which has no secular cooling of the mantle: the chemical cratonic root undergoes periodic dripping down up-welling over several 10s of Myr. The orange curves are isotherms for  $T = 1100\text{ }^{\circ}\text{C}$ ,  $1200\text{ }^{\circ}\text{C}$ ,  $1300\text{ }^{\circ}\text{C}$ ,  $1400\text{ }^{\circ}\text{C}$ , respectively. The dashed lines mark the depth of 200 km.

models as result of the thermal adjustment. This thermal adjustment also helps to stabilize the cratonic root, as discussed below. The thickening speed during this latter stage of craton evolution is significantly lower than in the first thickening stage as there is no external shortening imposed. Nonetheless, the cratonic root grows vertically by ~40 km during stage-2 thickening in our Reference Model R (Fig. 4), compared with ~43 km stage-1 thickening. This suggests that the two thickening stages may contribute equally to the total overall thickness of the cratonic lithosphere. The vertical movement of cratonic mantle material, which is implicit in these models, may be a way to generate specific aspects of the mineralogy of cratons, such as the presence of high-Cr, low-Ca knorringitic garnets that require low-pressure (<3 GPa) depleted

precursor lithologies that become subsequently pressurized to ~4 to 7 GPa (Canil and Wei, 1992; Stachel et al., 1998).

#### 4.2. Stabilization of cratons

Even though the high intrinsic viscosity and chemical buoyancy of the depleted root play important roles in the long-term stability of the cratons, our models show that the presence of a large amount of depleted mantle beneath continental crust material does not guarantee a stable craton. In the Reference Model R, the gravitational thickening stage is driven by the diffusive cooling of the root, and slowly embeds the chemically depleted root material within the thermal lithosphere, leading to a stable cratonic root (Fig. 2C–D). But if significantly more initial, tectonic shortening is applied (e.g. in Model SF3), the cratonic root (Fig. 4A) does not stabilize, and experiences continuous, significant basal erosion, even after long cooling periods. Therefore, rapid compressive shortening (10s of Myr) of a depleted mantle lithosphere alone may not form a stable thermo-chemical structure. Instead, a slow self-driven thickening and adjustment process, as a result of thermal equilibration (Schutt and Lesher, 2006), is required to stabilize the newly formed cratonic root. Within the context of our model parameters, the thickness of cratonic roots can be self-regulating and such a process may explain the relatively constant thickness of present-day cratonic roots.

Apart from an instability caused by large-scale tectonic shortening, our model results also illustrate another type of instability that can occur, as illustrated by Model SC2. In that case, cratonic root material becomes unstable and starts to oscillate on a timescale of a 10s of Myr (Fig. 8). Such oscillatory behaviour occurs after an initial, long quiet period of ~1.1 Gyr (Model SC2 in Fig. 7). This type of instability has previously been observed in other studies (Jaupart et al., 2007; Wang et al., 2015), and is different from a more commonly reported Rayleigh-Taylor style root collapse (e.g. Houseman and Molnar, 1997). A possible geological expression of this type of instability might be the complex temporal additions/modification of cratonic roots indicated by Re-Os isotopes and petrological studies of mantle xenoliths from the Rae craton, which appears to have experienced a considerably more complex evolutionary history than most cratons (Liu et al., 2016). Secular cooling is able to prevent the system from developing this oscillatory regime due to a combination of two effects. Firstly, the buoyancy number (ratio

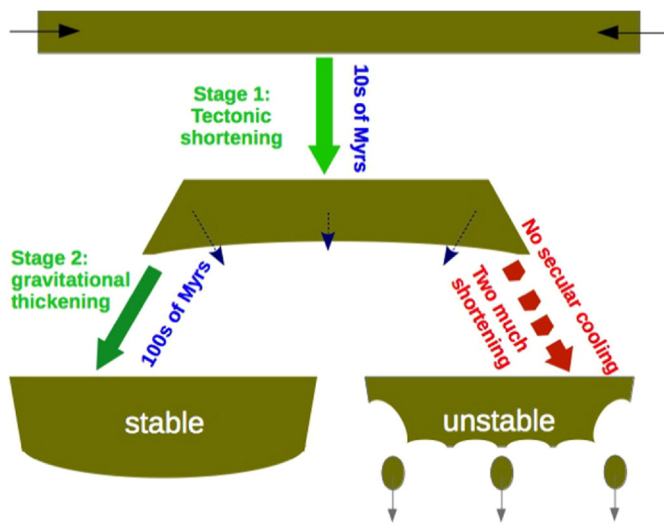


**Fig. 9.** The schematic diagram of the two-stage thickening model for the formation of thick cratons resulting from numerical simulations. The first stage of thickening is caused by tectonic shortening that last for 10s of Myr, while the second stage is driven by the gravity of the cooling root as a result of thermal equilibrium that lasts for 100s of Myr. A specific range of Stage 1 shortening (tectonic thickening) is required to introduce Stage 2 (gravitational thickening). Too much tectonic shortening may introduce an unstable root. In addition, mantle secular cooling also has a stabilizing effect on the cratonic root by preventing the oscillatory instability observed in Fig. 8.

between the compositional buoyancy and thermal buoyancy) is increased by reducing the temperature contrast during secular cooling. Secondly and perhaps more importantly, the Rayleigh number of the mantle convection is reduced as a result of the increase of background viscosity due to mantle cooling. Both of the two effects contribute to switching the system into a stable regime and leads to the stabilization of the cratonic root.

As a result of its long-term thermal evolution, a cratonic root that is approximately isopycnic under present conditions would have been either more or less buoyant in the past (Eaton and Claire Perry, 2013). This indicates that the long-term stability of cratons cannot simply be explained by a permanently isopycnic status, and that other contributions, for example from the high viscosity of the root (e.g. Wang et al., 2014) or secular cooling (Michaut et al., 2009), are essential to explain long-term cratonic root stability. On the basis of laboratory studies of the effects of melt depletion on the physical properties, Schutt and Leshner (2006) proposed another possible stabilization mechanism for cratons. Their experimental data argue that the depletion induced buoyancy for cratonic mantle that formed above 110 km is not enough to counteract the negative thermal buoyancy at their formation depth. Instead, the neutral buoyancy of the cratonic root might be achieved through thermal re-equilibrium after vertical transportation of the cratonic mantle and through thermal expansivity variation due to temperature and pressure changes. Such an effect, if taken into account in the geodynamical modelling, would potentially further promote the thickening and stabilization of cratonic root.

The models presented here have implications for the topographical evolution of cratons and their roots. In their early evolution, cratons witnessed dramatic subsidence, with the development, in some cases, of very large sedimentary basins, e.g., the 8 km thick Meso- to Neoproterozoic Witwatersrand basin of the central Kaapvaal craton (Robb & Meyer, 1995). McKenzie and Priestley (2016) have argued that the formation of intra-cratonic basins is a specific outcome of the thickening phase of cratons by lateral compression, if thick crust exists for a time-scale on the order of the thermal time constant of thick lithosphere and is then subsequently rapidly removed by erosion. In this sense, the lack of ability of our models to examine in detail the surface processes and crustal evolution accompanying craton formation are a weakness. The surface of the model domain is free-slip, which does not allow vertical motion as a response to mantle dynamics, and erosion and sedimentation processes are not considered. Also prograde metamorphism and densification of crust are not considered, so that delamination of eclogitic crust (e.g. Pearson and Wittig, 2008) does not occur. For now, the reader is referred to McKenzie and Priestley (2016) for a more detailed examination of the behaviour of the crust. Our models, instead, focus on the mantle part of the lithosphere as this portion is essential in maintaining the overall long-term integrity of a craton. To compensate for the secondary processes that tend to reduce crustal thickness, our models start with a relatively thin (20 km) crust. The crust forms only a relatively small fraction of the total craton, and we do not expect its effects on craton keel root development and underlying mantle dynamics to be significant. The complex metamorphic and structural evolution of young cratons are difficult to explore in our models in which topography can only be approximated through normal stresses on the top boundary. Evaluating the level of consistency between our models and these observations requires a detailed evaluation of the impact of the varying parameters in the models that will be explored elsewhere.

## 5. Conclusion

We performed numerical experiments to study the thickening and stabilization of cratonic roots in a thermally evolving mantle to explore a compressive thickening model for making thick cratonic roots (Jordan, 1978; McKenzie and Priestley, 2016). Our modelling results show a two-stage thickening and stabilization process, in which a layer of

depleted mantle (30–120 km) forms a thick cratonic root (>200 km) within a few 100 Myr. This process involves significant vertical movement of cratonic mantle material as an intrinsic part of the cratonization process, which agrees well with petrological observations (Canil and Wei, 1992; Lee and Chin, 2014) and geophysical arguments (Schutt and Leshner, 2006). Based on the geodynamical modelling, we suggest the following related key ingredients for the cratonization process: 1. Thickening of the cratonic root is initiated by a tectonic shortening phase that lasts for 10s of Myr and is followed by a gravitational thickening phase that lasts for 100s of Myr. 2. Initial tectonic shortening and thickening of previously depleted material occurs on length and time scales similar to modern orogenic tectonics (e.g. subduction accretion, lithosphere underplating, or continental collision), and is essential to initiate the cratonization process. 3. Gravitational self-thickening always follows initial tectonic compressive shortening and causes further thickening, while intrinsic compositional buoyancy prevents a Rayleigh-Taylor type collapse, and stabilizes the thick cratonic root. 4. Secular cooling of the ambient mantle has a stabilizing effect on the cratonic root by reducing the thermal buoyancy contrast between lithosphere and asthenosphere and increasing background viscosity, and forms an essential ingredient for the long-term survival of cratons.

## Acknowledgements

We would like to thank Thomas François, an anonymous reviewer, the Editor and Guest Editor for their constructive comments that helped to significantly improve the manuscript. We also thank Yaoling Niu for useful discussions. The data for this paper are available by contacting the corresponding author. The work has been supported by EU FP7 Marie Curie Initial Training Network 'Topomod' contract 264517. J.v.H. acknowledges funding from the European Research Council (ERC StG279828) and D.G.P. was supported by a Canada Excellence Research Chair.

## Appendix A. Supplementary data

Supplementary data to this article can be found online at <http://dx.doi.org/10.1016/j.tecto.2016.12.001>.

## References

- Arndt, N.T., Coltice, N., Helmstaedt, H., Gregoire, M., 2009. Origin of Archean subcontinental lithospheric mantle: some petrological constraints. *Lithos* 109 (1–2):61–71. <http://dx.doi.org/10.1016/j.lithos.2008.10.019>.
- Aulbach, S., 2012. Craton nucleation and formation of thick lithospheric roots. *Lithos* 149: 16–30. <http://dx.doi.org/10.1016/j.lithos.2012.02.011>.
- Bédard, J.H., Brouillette, P., Madore, L., Berclaz, A., 2003. Archean cratonization and deformation in the northern Superior Province, Canada: an evaluation of plate tectonic versus vertical tectonic models. *Precambrian Res.* 127 (1–3):61–87. [http://dx.doi.org/10.1016/S0301-9268\(03\)00181-5](http://dx.doi.org/10.1016/S0301-9268(03)00181-5).
- Burov, E.B., 2011. Rheology and strength of the lithosphere. *Mar. Pet. Geol.* 28 (8): 1402–1443. <http://dx.doi.org/10.1016/j.marpetgeo.2011.05.008>.
- Burov, E., Yamato, P., 2008. Continental plate collision, P-T-t conditions and unstable vs. stable plate dynamics: insights from thermo-mechanical modelling. *Lithos* 103 (1–2): 178–204. <http://dx.doi.org/10.1016/j.lithos.2007.09.014>.
- Canil, D., 2004. Mildly incompatible elements in peridotites and the origins of mantle lithosphere. *Lithos* 77:375–393. <http://dx.doi.org/10.1016/j.lithos.2004.04.014>.
- Canil, D., Wei, K., 1992. Constraints on the origin of mantle-derived low Ca garnets. *Contrib. Mineral. Petrol.* 109 (4):421–430. <http://dx.doi.org/10.1007/BF00306546>.
- Carlson, R.R.W., Pearson, D.G., James, D.D.E., 2005. Physical, chemical, and chronological characteristics of continental mantle. *Rev. Geophys.* (2004):1–24 <http://dx.doi.org/10.1029/2004RG000156>.
- Condie, K.C., Aster, R.C., van Hunen, J., 2016. A great thermal divergence in the mantle beginning 2.5 Ga: geochemical constraints from greenstone basalts and komatiites. *Geosci. Front.* 7 (4), 543–553.
- Cooper, C.M., Miller, M.S., 2014. Craton formation: internal structure inherited from closing of the early oceans. *Lithosphere* 6 (1):35–42. <http://dx.doi.org/10.1130/L321.1>.
- DeCelles, P.G., 2002. Implications of shortening in the Himalayan fold-thrust belt for uplift of the Tibetan Plateau. *Tectonics* 21 (6). <http://dx.doi.org/10.1029/2001TC001322>.
- Eaton, D.W., Claire Perry, H.K., 2013. Ephemeral isopycnicity of cratonic mantle keels. *Nat. Geosci.* 6 (11):967–970. <http://dx.doi.org/10.1038/ngeo1950>.
- Fei, H., Wiedenbeck, M., Yamazaki, D., Katsura, T., 2013. Small effect of water on upper-mantle rheology based on silicon self-diffusion coefficients. *Nature* 498 (7453): 213–215. <http://dx.doi.org/10.1038/nature12193>.

- Griffin, W.L., O'Reilly, S.Y., Abe, N., Aulbach, S., Davies, R.M., Pearson, N.J., Doyle, B.J., Kivi, K., 2003. The origin and evolution of Archean lithospheric mantle. *Precambrian Research*, vol. 127, pp. 19–41.
- Grove, T.L., Parman, S.W., 2004. Thermal evolution of the Earth as recorded by komatiites. *Earth Planet. Sci. Lett.* 219:173–187. [http://dx.doi.org/10.1016/S0012-821X\(04\)00002-0](http://dx.doi.org/10.1016/S0012-821X(04)00002-0).
- Gung, Y., Panning, M., Romanowicz, B., 2003. Global anisotropy and the thickness of continents. *Nature* 422 (April):707–711. <http://dx.doi.org/10.1038/nature01557.1>.
- Herzberg, C., 1999. Phase equilibrium constraints on the formation of cratonic mantle. *Mantle Petrology: Field Observations and High-pressure Experimentation*. Spec. Publ. *Geochem. Soc. No. 6*, pp. 241–257.
- Herzberg, C., Condie, K., Korenaga, J., 2010. Thermal history of the Earth and its petrological expression. *Earth Planet. Sci. Lett.* 292 (1–2):79–88. <http://dx.doi.org/10.1016/j.epsl.2010.01.022>.
- Hirth, G., Kohlstedt, D.L., 1996. Water in the oceanic upper mantle: implications for rheology, melt extraction and the evolution of the lithosphere. *Earth Planet. Sci. Lett.* 144 (1–2), 93–108.
- Hirth, G., Evans, R.L., Chave, A.D., 2000. Comparison of continental and oceanic mantle electrical conductivity: is the Archean lithosphere dry? *Geochem. Geophys. Geosyst.* 1 (12). <http://dx.doi.org/10.1029/2000GC000048>.
- Houseman, G.A., Molnar, P., 1997. Gravitational (Rayleigh–Taylor) instability of a layer with non-linear viscosity and convective thinning of continental lithosphere. *Geophys. J. Int.* 128 (1):125–150. <http://dx.doi.org/10.1111/j.1365-246X.1997.tb04075.x>.
- Jaupart, C., Molnar, P., Cottrell, E., 2007. Instability of a chemically dense layer heated from below and overlain by a deep less viscous fluid. *J. Fluid Mech.* 572:433. <http://dx.doi.org/10.1017/S0022112006003521>.
- Jordan, T., 1975. The continental tectosphere. *Rev. Geophys.* 13 (3).
- Jordan, T.H., 1978. Composition and development of the continental tectosphere. *Nature* 274 (5671):544–548. <http://dx.doi.org/10.1038/274544a0>.
- Karato, 2010. Rheology of the deep upper mantle and its implications for the preservation of the continental roots: a review. *Tectonophysics* 481 (1–4):82–98. <http://dx.doi.org/10.1016/j.tecto.2009.04.011>.
- Lee, C.-T.A., 2006. Geochemical/petrologic constraint on the origin of cratonic mantle. *Geophys. Monogr. Am. Geophys. Union* 164:89–114. <http://dx.doi.org/10.1029/164gm08>.
- Lee, C.-T.A., Chin, E.J., 2014. Calculating melting temperatures and pressures of peridotite protoliths: implications for the origin of cratonic mantle. *Earth Planet. Sci. Lett.* 403:273–286. <http://dx.doi.org/10.1016/j.epsl.2014.06.048>.
- Lee, C.-T.A., Luffi, P., Chin, E.J., 2011. Building and destroying continental mantle. *Annu. Rev. Earth Planet. Sci.* 39 (1):59–90. <http://dx.doi.org/10.1146/annurev-earth-040610-133505>.
- Liu, J., Riches, A.J.V., Pearson, D.G., Luo, Y., Kienlen, B., Kjarsgaard, B.A., Stachel, T., Armstrong, J.P., 2016. Age and evolution of the deep continental root beneath the central Rae craton, northern Canada. *Precambrian Res.* 272, 168–184.
- Mareschal, J.C., Jaupart, C., 2006. Archean thermal regime and stabilization of the cratons. *Archean Geodynamics and Environments*, vol. 164, pp. 61–73.
- McKenzie, D., Bickle, M.J., 1988. The volume and composition of melt generated by extension of the lithosphere. *J. Petrol.* 29 (3):625–679. <http://dx.doi.org/10.1093/ptrology/29.3.625>.
- McKenzie, D., Priestley, K., 2016. Speculations on the formation of cratons and cratonic basins. *Earth Planet. Sci. Lett.* 435:94–104. <http://dx.doi.org/10.1016/j.epsl.2015.12.010>.
- Michaut, C., Jaupart, C., 2007. Secular cooling and thermal structure of continental lithosphere. *Earth Planet. Sci. Lett.* 257 (1–2):83–96. <http://dx.doi.org/10.1016/j.epsl.2007.02.019>.
- Michaut, C., Jaupart, C., Mareschal, J.-C., 2009. Thermal evolution of cratonic roots. *Lithos* 109 (1–2):47–60. <http://dx.doi.org/10.1016/j.lithos.2008.05.008>.
- Moresi, L.-N., Solomatov, V.S., 1995. Numerical investigation of 2D convection with extremely large viscosity variations. *Phys. Fluids* 7 (9):2154–2162. <http://dx.doi.org/10.1063/1.868465>.
- Pearson, D.G.D., Wittig, N., 2008. Formation of Archean continental lithosphere and its diamonds: the root of the problem. *J. Geol. Soc. Lond.* 165 (5):895–914. <http://dx.doi.org/10.1144/0016-76492008-003>.
- Pearson, D.G., Wittig, N., 2014. The formation and evolution of cratonic mantle lithosphere - evidence from mantle xenoliths. *Treatise on Geochemistry*, second ed. vol. 3. Elsevier Ltd., pp. 255–292.
- Pearson, D., Carlson, R.W., Shirey, S.B., Boyd, F.R., Nixon, P.H., 1995. Stabilisation of Archean lithospheric mantle: a Re–Os isotope study of peridotite xenoliths from the Kaapvaal craton. *Earth Planet. Sci. Lett.* 134, 341–357.
- Priestley, K., McKenzie, D., 2013. The relationship between shear wave velocity, temperature, attenuation and viscosity in the shallow part of the mantle. *Earth Planet. Sci. Lett.* 381:78–91. <http://dx.doi.org/10.1016/j.epsl.2013.08.022>.
- Robb, L.J., Meyer, F.M., 1995. The Witwatersrand basin, South Africa: geological framework and mineralization processes. *Ore Geol. Rev.* 10, 67–94.
- Schutt, D.L., Leshar, C.E., 2006. Effects of melt depletion on the density and seismic velocity of garnet and spinel lherzolite. *J. Geophys. Res.* 111 (B5), B05401. <http://dx.doi.org/10.1029/2003JB002950>.
- Sizova, E., Gerya, T., Stüwe, K., Brown, M., 2015. Generation of felsic crust in the Archean: a geodynamic modeling perspective. *Precambrian Res.* 271:198–224. <http://dx.doi.org/10.1016/j.precamres.2015.10.005>.
- Sleep, N.H., 2005. Evolution of the continental lithosphere. *Annu. Rev. Earth Planet. Sci.* 33 (1):369–393. <http://dx.doi.org/10.1146/annurev.earth.33.092203.122643>.
- Stachel, T., Viljoen, K.S., Brey, G., Harris, J.W., 1998. Metasomatic processes in lherzolitic and harzburgitic domains of diamondiferous lithospheric mantle: REE in garnets from xenoliths and inclusions in diamonds. *Earth Planet. Sci. Lett.* 159 (1–2):1–12. [http://dx.doi.org/10.1016/S0012-821X\(98\)00064-8](http://dx.doi.org/10.1016/S0012-821X(98)00064-8).
- Tian, X., Liu, Z., Si, S., Zhang, Z., 2013. The crustal thickness of NE Tibet and its implication for crustal shortening. *Tectonophysics* 634:198–207. <http://dx.doi.org/10.1016/j.tecto.2014.07.001>.
- Toussaint, G., Burov, E., Jolivet, L., 2004. Continental plate collision: unstable vs. stable slab dynamics. *Geology* 32 (1):33–36. <http://dx.doi.org/10.1130/G19883.1>.
- van Hunen, J., Allen, M.B., 2011. Continental collision and slab break-off: a comparison of 3-D numerical models with observations. *Earth Planet. Sci. Lett.* 302 (1–2):27–37. <http://dx.doi.org/10.1016/j.epsl.2010.11.035>.
- van Hunen, J., van den Berg, A.P., 2008. Plate tectonics on the early Earth: limitations imposed by strength and buoyancy of subducted lithosphere. *Lithos* 103 (1–2):217–235. <http://dx.doi.org/10.1016/j.lithos.2007.09.016>.
- van Hunen, J., Zhong, S., Shapiro, N.M., Ritzwoller, M.H., 2005. New evidence for dislocation creep from 3-D geodynamic modeling of the Pacific upper mantle structure. *Earth Planet. Sci. Lett.* 238:146–155. <http://dx.doi.org/10.1016/j.epsl.2005.07.006>.
- Wang, H., van Hunen, J., Pearson, D.G., Allen, M.B., 2014. Craton stability and longevity: the roles of composition-dependent rheology and buoyancy. *Earth Planet. Sci. Lett.* 391:224–233. <http://dx.doi.org/10.1016/j.epsl.2014.01.038>.
- Wang, Y., Huang, J., Zhong, S., 2015. Episodic and multi-staged gravitational instability of cratonic lithosphere and its implications for reactivation of the North China Craton. *Geochim. Geophys. Geosyst.*:815–833 <http://dx.doi.org/10.1002/2014GC005681>.
- Wittig, N., Pearson, D.G., Webb, M., Ottley, C.J., Irvine, G.J., Kopylova, M., Jensen, S.M., Nowell, G.M., 2008. Origin of cratonic lithospheric mantle roots: a geochemical study of peridotites from the North Atlantic Craton, West Greenland. *Earth Planet. Sci. Lett.* 274:24–33. <http://dx.doi.org/10.1016/j.epsl.2008.06.034>.
- Zhong, S., Zuber, M.T., Moresi, L., Michael, G., 2000. Role of temperature-dependent viscosity and surface plates in spherical shell models of mantle convection. *J. Geophys. Res.* 105 (B5):11063–11082. <http://dx.doi.org/10.1029/2000JB900003>.